APPLIED GEOPHYSICS, Vol.10, No.2 (June 2013), P. 181-190, 18 Figures.
DOI: 10.1007/s11770-013-0380-6

Geophysical data sparse reconstruction based on *L0*-norm minimization*

Chen Guo-Xin[1], Chen Sheng-Chang[1♦], Wang Han-Chuang[1], and Zhang Bo[1]

Abstract: Missing data are a problem in geophysical surveys, and interpolation and reconstruction of missing data is part of the data processing and interpretation. Based on the sparseness of the geophysical data or the transform domain, we can improve the accuracy and stability of the reconstruction by transforming it to a sparse optimization problem. In this paper, we propose a mathematical model for the sparse reconstruction of data based on the *L0*-norm minimization. Furthermore, we discuss two types of the approximation algorithm for the *L0*-norm minimization according to the size and characteristics of the geophysical data: namely, the iteratively reweighted least-squares algorithm and the fast iterative hard thresholding algorithm. Theoretical and numerical analysis showed that applying the iteratively reweighted least-squares algorithm to the reconstruction of potential field data exploits its fast convergence rate, short calculation time, and high precision, whereas the fast iterative hard thresholding algorithm is more suitable for processing seismic data, moreover, its computational efficiency is better than that of the traditional iterative hard thresholding algorithm.
Keywords: Geophysical data, sparse reconstruction, *L0*-norm minimization, iteratively reweighted least squares, fast iterative hard thresholding

Introduction

In geophysical data acquisition, data are often incomplete and irregular because of poor field conditions, equipment failure, and noise. However, various kinds of geophysical data processing methods, such as the continuation of the potential field, and seismic data migration and inversion, require complete data sets (Wang et al., 2011). Incomplete data cause loss of information, and subsequently introduce noise in the data processing and lower the quality of the results (Meng et al., 2012). Thus, data reconstruction is a significant problem in geophysical data processing and interpretation.

Reconstruction methods differ for data sets of different size and characteristics. For potential field data, the reconstruction methods mainly include the linear interpolation method, the spline function method, and the inverse interpolation method (Guo et al., 2005), whereas the reconstruction of seismic data is mostly based on transform methods such as the Fourier transform (Duijndam et al., 1999; Liu et al., 2004) and the radon transform (Trad et al., 2003), which use the characteristics of the data in the transform domain. However, regardless of the type of data, the reconstruction of incomplete data sets is an ill-posed inverse problem that requires regularization constraints to ensure the stability of the solution. *L2*-norm minimization algorithms, such as the Tikhonov regularization method (Tikhonov and Arsenin, 1977),

Manuscript received by the Editor January 24, 2013; revised manuscript received May 1, 2013.
*This work was supported by the National Natural Science Foundation of China (Grant No. 41074133).
1. Department of Earth Sciences, Zhejiang University, Hangzhou 310027, China.
♦Corresponding Author: Chen Sheng-Chang (Email: chenshengc@zju.edu.cn)

are commonly used. General quadratic constraints can also effectively improve the stability of algorithms with continuous solutions, but it smooth the discontinuous features of the data, thus reducing the resolution of the inversion results.

In order to guarantee the stability and accuracy of the solutions, geophysicists used the optimization algorithms based on *L0*-norm minimization to analyze seismic reflection data (Levy and Fullagar, 1981). Presently, sparse optimization algorithms are widely used in seismic data reconstruction and denoising (Tang and Yang, 2010; Cao et al., 2012; Tang et al., 2012), the deconvolution of poststack seismic data, wave impedance inversion (Pei, 2009), full waveform inversion (Li, a., 2012), and others. Because the *L0*-norm is a measure of data sparsity, the *L0*-norm minimization is the optimum sparse optimization algorithm; however, it is a combinatorial optimization for directly solving the problem without a polynomial time solution. Donoho et al. (2012) proved that the solutions of the *L1*-norm minimization and the *L0*-norm minimization are equivalent when the measurement matrix satisfies certain constraint conditions. The *L1*-norm minimization differs from the *L0*-norm minimization and has many direct solution methods. Nonetheless, the equivalent decision conditions are complex and the solutions of the algorithm cannot locate the sparse coefficient (Jiao et al., 2011). Though it is difficult to directly solve the *L0*-norm minimization, we can avoid complicated calculations for the equivalent conditions of the decision operation in the *L1*-norm minimization algorithm with better approximate solution methods, and solve the problem of the sparse coefficient position confusion. There are many approximate solution methods. Greedy algorithms such as the matching pursuit algorithm (Mallat and Zhang, 1993; Tropp and Gilbert, 2007) with low computational complexity and high-speed computational capability have been widely applied. However, low computation precision and poor antinoise ability make them unsuitable for the reconstitution of less sparse data. The hard iterative thresholding (HIT) algorithm is simple and suitable for large-scale data processing, its shortcoming is that the convergence rate is too slow (Blumensath and Davies, 2009). To improve the convergence rate of the HIT algorithm, many accelerated iteration methods were proposed, such as the regularized HIT method (Blumensath and Davies, 2010), the expectation–conditional maximization either (ECME) algorithm (Qiu and Dogandzic, 2010), the two-step iterative shrinkage–thresholding (IST) algorithm (Bioucas-Dias and Figueired, 2007), etc. These algorithms, however, need harsh conditions or do not guarantee convergence (Blumensath, 2012).

In this paper, we discuss a geophysical data sparse reconstruction mathematical model based on the *L0*-norm minimization and introduce two approximation algorithms for the *L0*-norm minimization according to the different size and characteristics of the data; namely, the iteratively reweighted least-squares (IRLS) algorithm based on the *L0*-norm minimization and the fast iterative hard thresholding (FIHT) algorithm with fast convergence rate. We also show with numerical experiments that the two algorithms have low computational complexity, fast convergence rate, and high accuracy.

Methods and principles

Geophysical data sparse reconstruction modeling based on *L0*-norm minimization

According to the compressed sensing theory proposed by Candes and Wakin (2006), and Donoho et al. (2006), the collection of geophysical data can be viewed as a projection process

$$\mathbf{Y} = \mathbf{AX} + \mathbf{e}\,, \tag{1}$$

where $\mathbf{A}$ is the projection matrix (M*N, $M < N$), namely the observation matrix, and $\mathbf{X} \in R^N$ represents the original regular geophysical data. Through the projection matrix $\mathbf{A}$, the high-dimensional data in $\mathbf{X}$ are mapped in the low-dimensional space (M dimension) from the high-dimensional space (N dimension) to obtain $\mathbf{Y}$. The latter is the incomplete measured data ($\mathbf{Y} \in R^N$), and $\mathbf{e} \in R^M$ is the noise. The corresponding geophysical data reconstruction is an inverse problem of projection, which uses the low-dimensional observation data $\mathbf{Y}$ and the projection matrix $\mathbf{A}$ to retrieve the original data $\mathbf{X}$ in high-dimensional data space by solving the least-squares problem

$$\min \left\| \mathbf{Y} - \mathbf{AX} \right\|_2^2 . \tag{2}$$

Because $M < N$, equation (1) is an underdetermined system of equations; therefore, equation (2) is an ill-posed problem. The correctness of the solution cannot be guaranteed by directly solving equation (2). If $\mathbf{X}$ is sparse or the transform coefficients in the transform domain are sparse, then the data reconstruction can be converted into a sparse optimization problem. As a result, we need to convert $\mathbf{X}$ to the transform domain

$$\mathbf{X} = \mathbf{\Psi\Theta}, \quad (3)$$

where $\mathbf{\Psi}$ is the transform operator, and the concrete form is decided by using the transform method. $\mathbf{\Theta}^T = [\theta_1, \theta_2, \ldots, \theta_i, \ldots, \theta_N]$ are the transform coefficients in the transform domain. $\mathbf{X}$ and $\mathbf{\Theta}$ are equivalent representations of $\mathbf{X}$ in the time–space and transform domains. If most elements of $\mathbf{\Theta}$ are zero, $\mathbf{\Theta}$ is sparse, and the corresponding transformation is called the sparse transformation of $\mathbf{X}$. Using the *L0*-norm minimization as the objective function, the reconstruction of geophysical data can be transformed into the *L0*-norm minimization based on the sparse optimization

$$\min \left\| \mathbf{\Theta} \right\|_0 \quad \text{s.t.} \left\| \mathbf{Y} - \mathbf{A\Psi\Theta} \right\|_2^2 \le \varepsilon, \quad (4)$$

where $||\mathbf{\Theta}||_0$ is the *L0*-norm of $\mathbf{\Theta}$, i.e., the measure of sparseness.

There are two prerequisites for solving the sparse optimization problem and obtain accurately reconstructed data. First, we have to design an efficient observation matrix $\mathbf{A}$. Traditional regular undersampling will generate coherent aliasing, which affects the quality of the results. Although random undersampling methods can convert coherent aliasing to signal-independent noise, they cannot control the sampling interval, leaving behind sampling redundancies or deficiencies. Poisson sampling (Dunbar and Humphreys, 2006) and the jitter sampling method (Hennenfen and Herrmann, 2008) have found wide use in image processing and can even the sampling points as possible under the conditions of random sampling. Sampling data with blue-noise spectrum characteristics can improve the quality of the reconstruction data. Second, we need to choose a suitable sparse transform operator $\mathbf{\Psi}$ to sparsely represent $\mathbf{X}$. For greater sparse data representation and accurate reconstruction, less observation data are needed. The sparse transform method should be chosen according to the specific data characteristics. A method that is suitable for one type of data is not necessarily suitable for another type of data. In light of the geophysical data specifics, it is better to choose the Fourier transform or cosine transform for the potential field data, because of good continuity and slow change. Seismic data consist of complex curve elements. Thus, the wavelet and curvelet transforms, which have time–frequency local analysis ability (Candès and Donoho, 2000; Herrmann and Hennenfent, 2008), should be chosen. The curvelet transform has primitive curve shapes. It maintains the traditional wavelet multiscale features, and also has directivity and anisotropy. Thus, it is more suitable for sparse representation of the singular characteristics of two-dimensional curves and is a good choice for the seismic data sparse transform.

The sparse reconstruction algorithms based on *L0*-norm minimization

Iteratively reweighted least squares (IRLS)

The Lagrange multiplier method is used to transform equation (4) into an unconstrained optimization problem

$$\min \left\| \mathbf{Y} - \mathbf{A\Psi\Theta} \right\|_2^2 + \lambda \left\| \mathbf{\Theta} \right\|_0, \quad (5)$$

where $\lambda > 0$ is the Lagrange multiplier. Equation (5) is a nonconvex problem with no analytical solution. However, borrowing the IRLS algorithm and introducing a weight coefficient matrix $\mathbf{W}$, we can have $\left\| \sqrt{\mathbf{W}}\mathbf{\Theta} \right\|_2^2$ as approximate expression of the $||\mathbf{\Theta}||_0$. The diagonal weight coefficient matrix is $\mathbf{W} = \mathrm{diag}\left(\omega_1, \omega_2, \omega_3, ..\omega_N\right)$ and the diagonal elements ω_i are iteratively updated according to the θ_i solution

$$\omega_i^{t+1} = \left(\left(\theta_i^t \right) + \varepsilon \right)^{-1}, \quad (6)$$

where t is the number of iterations and ε is a small numerical parameter; thus, preventing the overflow of the right-hand side of equation (6).

We substitute equation (6) into $\left\| \sqrt{\mathbf{W}}\mathbf{\Theta} \right\|_2^2$ and if the algorithm is convergent, then $\left\| \sqrt{\mathbf{W}}\mathbf{\Theta} \right\|_2^2 \to \left\| \mathbf{\Theta} \right\|_0$. By iteratively solving the following regularized least-squares problem, we can solve equation (5) using equation (7)

$$\min \left\| \mathbf{Y} - \mathbf{A\Psi\Theta} \right\|_2^2 + \lambda \left\| \sqrt{\mathbf{W}}\mathbf{\Theta} \right\|_2^2. \quad (7)$$

Typical methods for solving the extreme-value problem may be used to solve equation (7), i.e., $\partial \mathrm{L}(\mathbf{\Theta})/\partial\mathbf{\Theta} = 0$. The analytical expressions of the optimal solution can be obtained from

$$\mathbf{\Theta} = \mathbf{W}\left(\mathbf{A\Psi}\right)^T \left(\mathbf{A\Psi W}\left(\mathbf{A\Psi}\right)^T + \lambda \mathbf{I} \right)^{-1} \mathbf{Y}. \quad (8)$$

In applying the algorithm, the specific steps of the iterative process are the following:

- Let the initial value of the t iteration be zero and make the initial value of the weight coefficient matrix $\mathbf{W}$ the unit matrix.
- Substitute the corresponding $\mathbf{A}$, $\mathbf{\Psi}$, and $\mathbf{\Theta}$ into equation (8) and iteratively obtain the solution $\mathbf{\Theta}'$ of the t iteration.
- Use the solution of the t iteration to update the weight coefficient matrix

$$\mathbf{W}^{t+1} = \mathrm{diag}\left(\omega_1^{t+1}, \omega_2^{t+1}, \omega_3^{t+1}, ...\omega_N^{t+1}\right),$$
$$\omega_i^{t+1} = \left(\left(\theta_i^t\right)^2 + \varepsilon\right)^{-1}. \quad (9)$$

- If $\left\|\mathbf{\Theta}^{t+1} - \mathbf{\Theta}^t\right\|_2^2 \le \delta$ or the number of iterations t exceeds the maximum number of iterations T, stop the iteration.
- Finally, the data reconstruction is $\mathbf{X} = \mathbf{\Psi\Theta}$.

Fast iterative hard thresholding (FIHT)

When faced with massive data sets, the IRLS algorithm requires high-dimensional matrix inversion. This kind of operation is quite complex and time-consuming. Therefore, the IRLS algorithm is not suitable for large-scale data processing. The FIHT algorithm, which is based on the *L0*-norm minimization via continuous iterative corrections, can avoid the inverse operation of high-order matrices. The solution formula of the FIHT algorithm is simple and generally of the form

$$\mathbf{\Theta}^{n+1} = \mathrm{H}_{\mathrm{K}}\left(\mathbf{\Theta}^n + \left(\mathbf{A\Psi}\right)^T\left(\mathbf{Y} - \mathbf{A\Psi\Theta}^n\right)\right), \quad (10)$$

where n is the number of iterations and $\mathrm{H}_{\lambda t}$ is the thresholding operator that is expressed as

$$\mathrm{H}_{\lambda t}\left(\Theta\right) = \begin{cases} \theta_i, \left|\theta_i\right| > \lambda t \\ 0, \left|\theta_i\right| < \lambda t \end{cases}, \quad (11)$$

where λt is the threshold. The FIHT algorithm is widely used in various fields because of its low computational complexity. Nonetheless, the algorithm also has the same shortcomings as other iterative thresholding algorithms, namely, slow convergence rate.

To overcome the slow convergence rate of the traditional iterative thresholding (TIT) algorithms, Beck and Teboulle (2009) presented the fast iterative shrinkage-thresholding algorithm based on *L1*-norm minimization. In this algorithm, the nth iteration result is the optimum combination of the (n−1)th and (n−2)th iteration solutions, and the combination coefficient is calculated using the optimization algorithm. Compared with the sublinear global convergence of the traditional iterative shrinkage−thresholding algorithm, the convergence rate of FIST is greatly improved

$$\mathrm{F}\left(\mathbf{\Theta}^n\right) - \mathrm{F}\left(\mathbf{\Theta}^*\right) \approx \mathrm{O}\left(\frac{1}{n^2}\right) \left(\mathrm{F}\left(\mathbf{\Theta}\right) = \left\|\mathbf{Y} - \mathbf{A\Psi\Theta}\right\|_2^2\right) + \lambda\left\|\mathbf{\Theta}\right\|_0, \quad (12)$$

where n is the number of iterations and $\mathbf{\Theta}^*$ is the global optimal solution.

We used the accelerated FIST and iterative hard thresholding (IHT) algorithms to obtain the fast iterative hard thresholding (FIHT) algorithm for solving the *L0*-norm minimization problem. The iteration process of the algorithm is

$$\mathbf{\Theta}^0 = \vec{0},$$
$$\mathbf{\Theta}^1 = \mathrm{H}_{\lambda t}\left(\mathbf{\Theta}^0 + \mu_1\left(\mathbf{A\Psi}\right)^T\left(\mathbf{Y} - \mathbf{A\Psi\Theta}^0\right)\right),$$
$$\mathbf{Z}^{n+1} = \mathbf{\Theta}^n + \frac{a^n - 1}{a^{n+1}}\left(\mathbf{\Theta}^n - \mathbf{\Theta}^{n-1}\right), \quad n \ge 1,$$
$$\mathbf{\Theta}^{n+1} = \mathrm{H}_{\lambda t}\left(\mathbf{Z}^{n+1} + \mu_{n+1}\left(\mathbf{A\Psi}\right)^T\left(\mathbf{Y} - \mathbf{A\Psi Z}^{n+1}\right)\right), \; n \ge 1,$$
$$a^{n+1} = \left(1 + \sqrt{1 + 4\left(a^n\right)^2}\right)\Big/2 \quad , a_0 = 1, n \ge 0,$$
$$\mu_{n+1} = \frac{\left\|\left(\mathbf{A\Psi}\right)^T\left(\mathbf{Y} - \mathbf{A\Psi\Theta}^n\right)\right\|_2^2}{\left\|\mathbf{A\Psi}\left(\mathbf{A\Psi}\right)^T\left(\mathbf{Y} - \mathbf{A\Psi\Theta}^n\right)\right\|_2^2} \quad n \ge 0,$$
$$\lambda t = T0 * a^n, \quad n \ge 0, \quad 0 < a < 1. \quad (13)$$

Unlike the traditional iterative hard thresholding algorithm, the nth iteration values in the FIHT algorithm is the optimum combination of the $(n-1)^{\mathrm{th}}$ and $(n-2)^{\mathrm{th}}$ iteration solutions to improve the stability of the algorithm. The optimization algorithm is used to retrieve the optimum step of the iterations and to accelerate the convergence rate. The threshold value λt is the correlation function containing the initial threshold *T0*, attenuation factor a, and number of iterations n. Adjusting *T0* and the attenuation factor a in terms of the amplitude of the data variations can also speed up the algorithm convergence rate.

Numerical experiments

Potential field data sparse reconstruction experiments

To evaluate the sparse reconstruction algorithms proposed in this paper, we applied them to the reconstruction of actual geophysical data. First, we used field data to test the application effect of the algorithms. Figure 1 shows gravity anomaly data of a region in the Sichuan province. There are 59 measuring lines, 125 points in each line, a total of 7375 observation points, the spacing between the observation points is 50 m, and the amplitude of the data is between 280 and 340 mGal. We used Poisson sampling for the 2000 sampling

points. The distribution of the sampling points is shown in Figure 2 and the corresponding frequency spectrum in Figure 3. As shown in Figure 2, the sampling points are distributed randomly and uniformly. There are no redundancies or deficiencies in the sampling area. Figure 3 exhibits typical blue-noise frequency spectrum characteristics and no coherent aliasing is produced by regular undersampling.

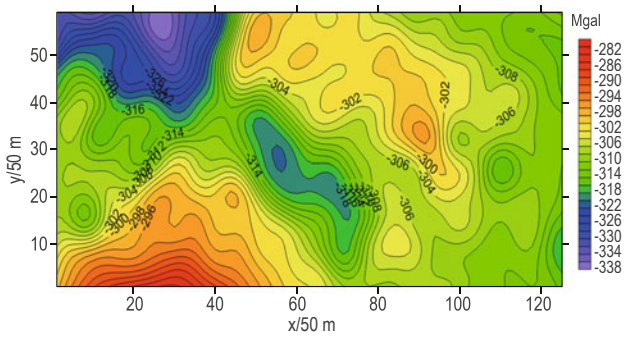

Fig.1 Contour map of the original data.

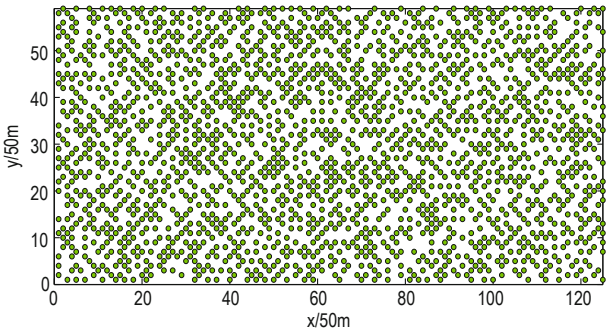

Fig.2 Sample distribution of Poisson sampling.

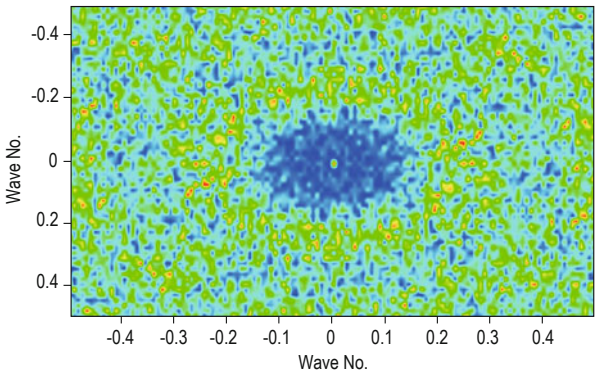

Fig.3 Frequency spectrum of the data from Poisson sampling.

Under the condition of unchanged random sampling, we respectively applied the iteratively reweighted least-squares and fast iterative hard thresholding algorithm to reconstruct the incomplete sampling data set. To compare the effect of the algorithms, we used the reconstruction results of the orthogonal matching pursuit algorithm and the iterative hard thresholding algorithm. According to the spatial variation characteristics of the potential field data, these algorithms use the discrete cosine transform as the sparse transform method. Table 1 lists the calculation time, mean square error (MSE) and the relative error (RE) of the different algorithms, and the corresponding diagrams.

Table 1 Recovery results according to different methods

Algorithms	Calculation Time (s)	MSE (10^{-3} gal)	RE	Results	Error
IRLS	452.9	0.3377	$6.73*10^{-4}$	Figure 4a	Figure 4b
FIHT	1680.7	0.3840	$7.29*10^{-4}$	Figure 5a	Figure 5b
OMP	269.6	1.6295	$3.28*10^{-3}$	Figure 6a	Figure 6b
IHT	5112.4	1.3648	$2.94*10^{-3}$		

According to Table 1 and the corresponding diagrams, the IRLS and FIHT algorithms are superior to the OMP and IHT algorithms based on the accuracy of the calculations. Regardless of the MSE magnitude

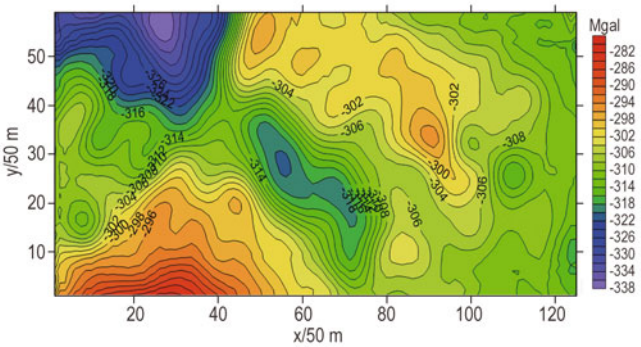

Fig.4a Contour map of the IRLS reconstruction results.

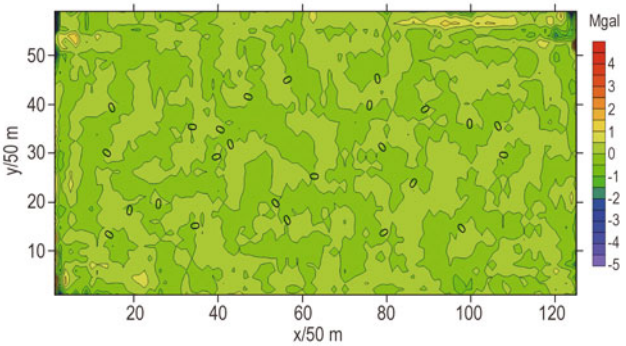

Fig.4b Contour map of the IRLS reconstruction error.

or the RE magnitude, the first two algorithms are one order lower than the other two algorithms. As shown in Figures 4a and 5b, most of the fitting error in the reconstructed and original data is near zero, except near the edges because of boundary effects. In terms of computation time, the IRLS is slightly longer than the OMP. Even though the FIHT is slower than the IRLS, its computation time is less than a third of the IHT, proving the correctness and efficiency of the FIHT acceleration strategy. The computation time of the OMP algorithm is the shortest of the four algorithms but its antinoise ability is low. Furthermore, the accuracy of the reconstruction results (Figures 6a and 6b) is low. The advantage of the low computation time of the OMP algorithm relative to the IRLS and FIHT is not enough to compensate for the low precision of the calculations.

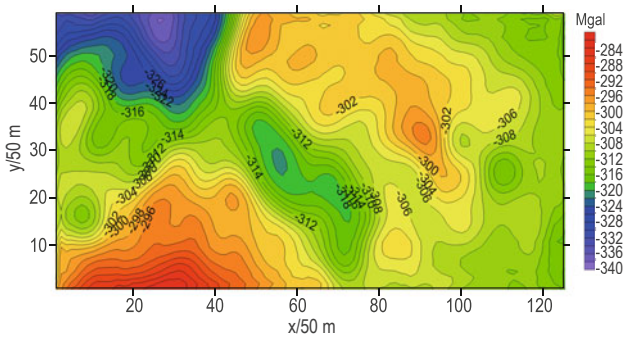

Fig.5a Contour map of the FIHT reconstruction results.

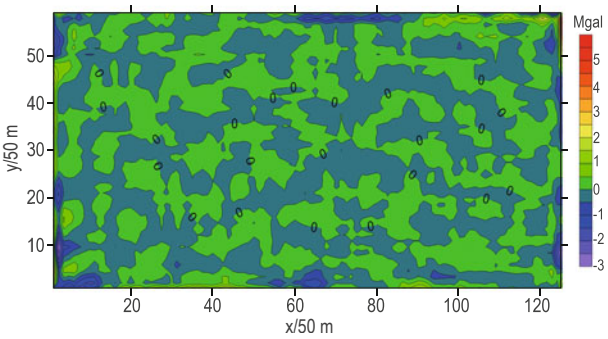

Fig.5b Contour map of the FIHT reconstruction error.

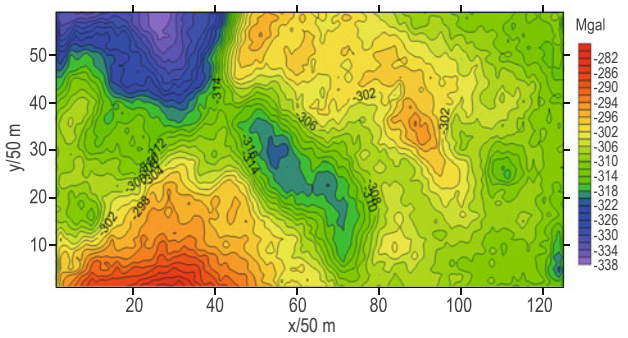

Fig.6a Contour map of the OMP reconstruction results.

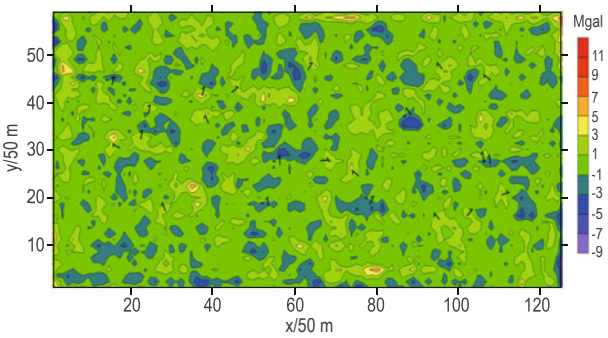

Fig.6b Contour map of the OMP reconstruction error.

To further compare the performance of the various algorithms in the reconstruction of potential field data, we also considered the iterative convergence curves of the IRLS algorithm, the FIHT algorithm, the OMP algorithm, and the IHT algorithm. Figure 7 shows the number of iterations on the horizontal axis and the vertical axis is the logarithm of relative error $\log_{10}(\|x - \tilde{x}\|_2^2 / \|x\|_2^2)$. As shown in the iterative convergence curve, the IRLS algorithm has the fastest convergence rate. Relative to the IHT algorithm, the convergence rate of the FIHT algorithm is better and can sooner meet the termination conditions of the algorithm. The OMP algorithm convergence rate is initially fast and the relative error is low; however, in the subsequent iterations, the convergence speed is very slow and attenuates to zeros fastly. Therefore, subsequent iterations do not improve the reconstruction precision of the data.

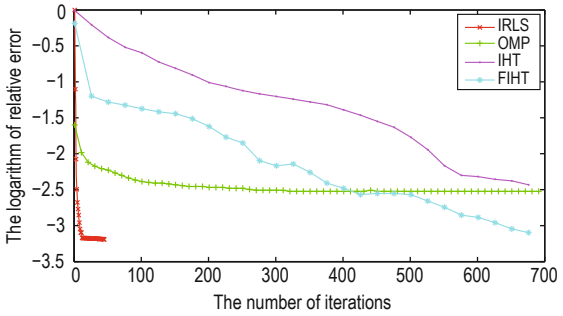

Fig.7 Iterative convergence curves of the algorithms used in the reconstruction of the potential field data.

Seismic data sparse reconstruction experiments

In small-scale and gentle-change potential field data reconstruction experiments, the computational efficiency and accuracy of the IRLS algorithm are superior to those of the FIHT algorithm. However, the IRLS algorithm is not suitable for large-scale seismic

data sparse reconstruction because it involves the direct inverse matrix and sparse transform, such as the curvelet transform, which is well suited for the sparse expression of seismic data that cannot be written in matrix form.

To test the effectiveness of the FIHT algorithm in seismic data reconstruction, first of all, we applied the algorithm to simulate simple seismogram reconstruction experiments, using the curvelet transform for the sparse representation of the seismic data. Figure 8 is a simulated seismic record. The spatial sampling interval is 10 m and the time sampling interval is 0.5 ms. Figures 9 and 10 respectively show the sampling data and diagram obtained by using the Poisson sampling method. The sampling data are half of the total data. The data sampling interval in Figure 9 is uniform, without being too large or too small. From the diagram, we can also see that Poisson sampling avoids coherent aliasing arising from regular undersampling and guarantees the reconstruction accuracy of the data. For the FIHT algorithm, the number of iterations was 56, the computation time was 325.6 s, the signal-to-noise ratio was 24.65 dB, and the mean square error was 0.0034. Figures 11 and 12 respectively show the reconstruction results and error. As shown in Figure 11, the seismic data reconstruction results well agree with the original data and there are deviations where the change in the data amplitude is intense. The experimental results show that either the SNR or the quality of the results is satisfactory. Compared with the traditional iterative hard thresholding algorithm, the number of iterations decreased from hundreds to dozens, thus, minimizing the computation time.

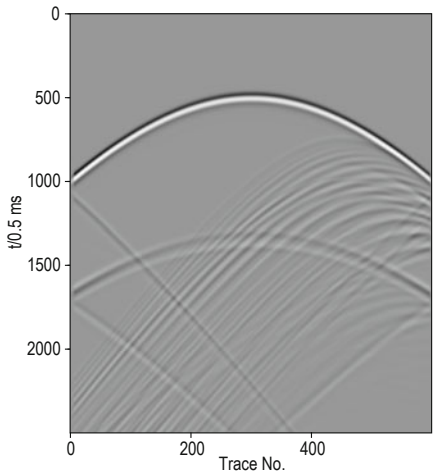

Fig.8 Original simulation seismic data.

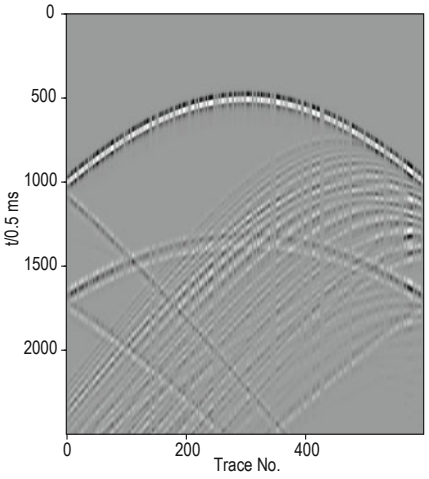

Fig.9 Irregular seismic data by Poisson sampling.

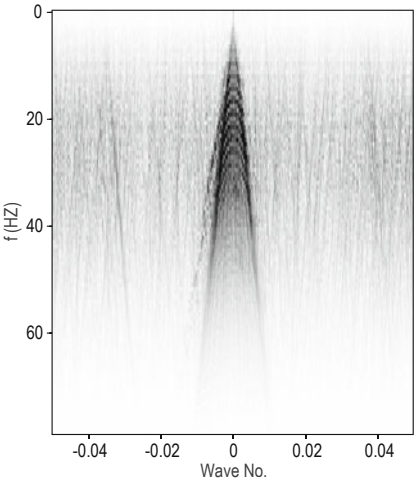

Fig.10 Frequency spectrum of the irregular seismic data by Poisson sampling.

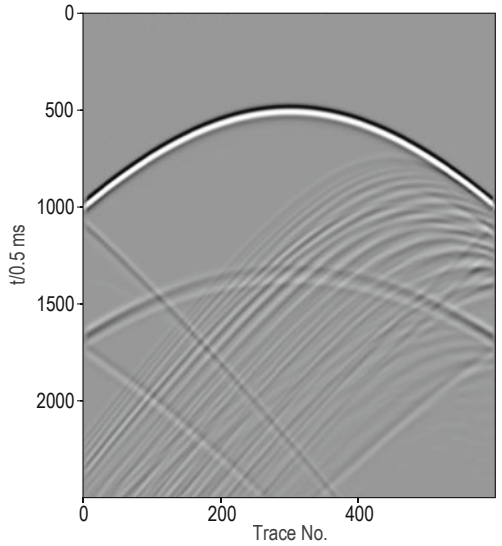

Fig.11 Reconstruction results of the FIHT algorithm.

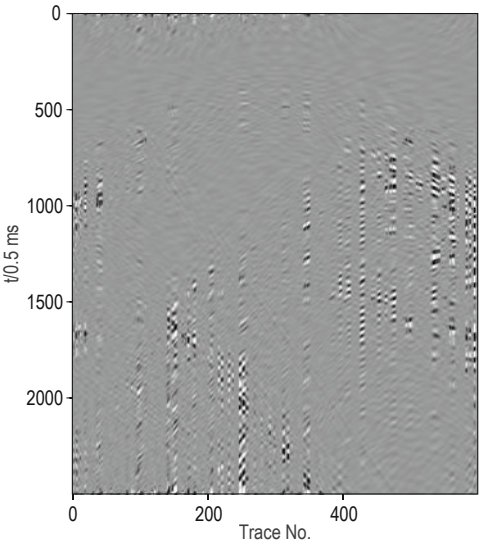

Fig.12 Reconstruction error of the FIHT algorithm.

To further examine the algorithms' performance in complex data reconstruction, we adopted the poststack seismic data of the international general 2D SEG/EAGE salt dome model (Figure 13) to test the FIHT algorithm. For comparison, we also tested the fast iterative shrinkage–thresholding algorithm. For the Poisson sampling method, the sampling results and the corresponding spectrum are shown in Figures 14 and 15. From Figure 15 we can see that Poisson sampling transforms the coherent aliasing because of regular undersampling into irrelevant random noise, which meets the prerequisites for data sparse reconstruction. We also adopted the curvelet transform and improved the algorithm convergence rate by adjusting the iterative format, the iteration step length μ, the initial threshold $T0$, and the attenuation factor a. After 63 iterations, the fast iterative shrinkage–thresholding algorithm meets the accuracy requirements of the solution. The computation time was 854.9 s, the relative error was 0.1407, and the signal-to-noise ratio was 8.51 dB.

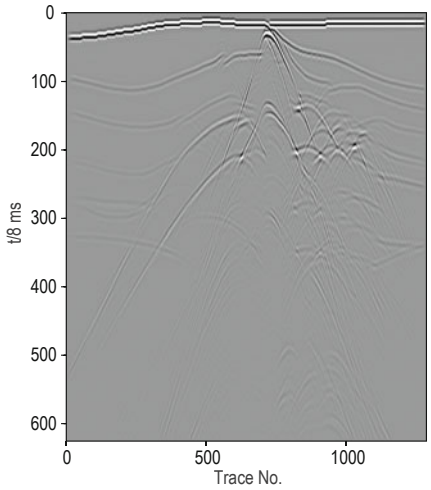

Fig.13 The 2D poststack seismic data of the SEG/EAEG salt velocity model.

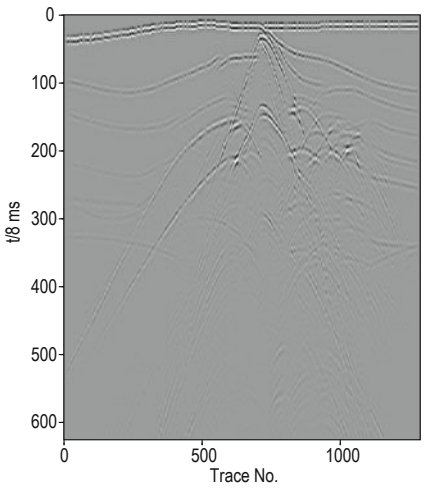

Fig.14 Irregular seismic data by Poisson sampling.

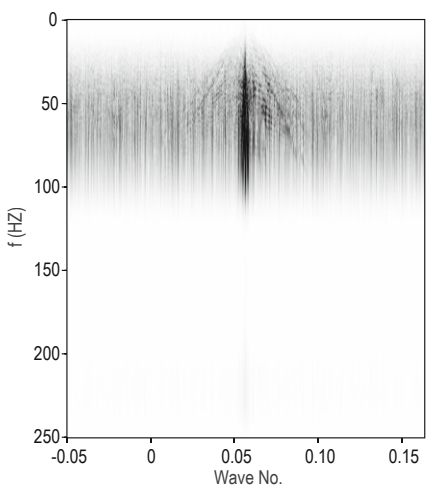

Fig.15 Frequency spectrum of irregular seismic data by Poisson sampling.

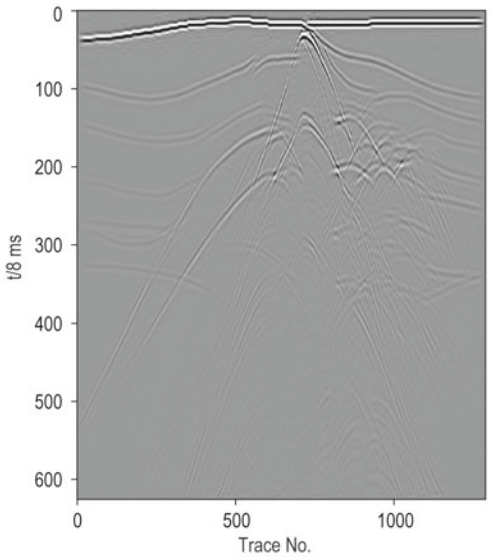

Fig.16a Reconstruction results of the fast iterative hard thresholding algorithm.

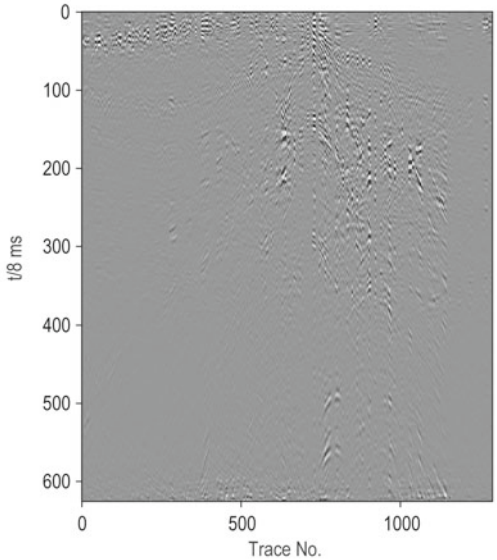

Fig.16b Reconstruction error of the fast hard iterative hard thresholding algorithm.

Figures 16a, 16b, 17a, and 17b respectively show the reconstruction results and error of the FIHT and FIST algorithms. As shown in Figure 16a, the vast majority of the poststack seismic data produced accurate reconstruction results, regardless of the deviations in the boundaries or regions where the data amplitude change is intense. This demonstrates the effectiveness and practicability of the FIHT algorithm. In contrast, the reconstruction effect of the FIHT algorithm is better than the FIST algorithm, for the reconstructed data show better continuity.

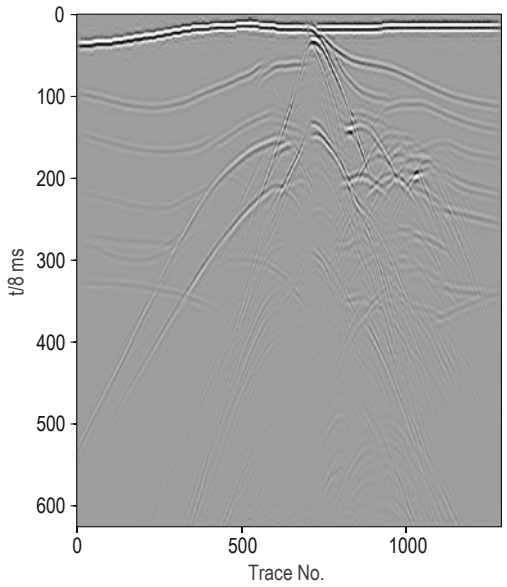

Fig.17a Reconstruction results of the fast iterative shrinkage–thresholding algorithm.

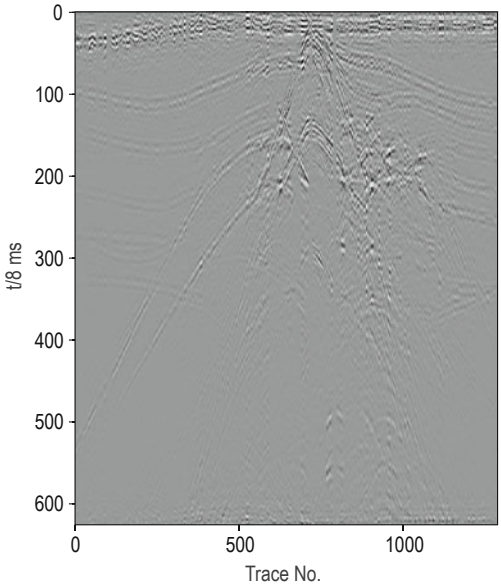

Fig.17b Reconstruction error of the fast iterative shrinkage–thresholding algorithm.

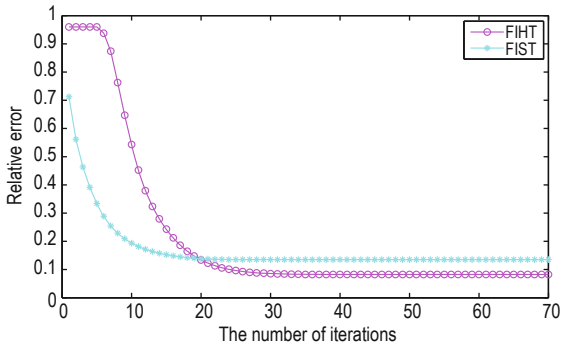

Fig.18 Iterative convergence curves of the algorithms used in the reconstruction of the 2D poststack seismic data of SEG/EAEG salt velocity model.

Figure 18 shows the convergence curve of the two kinds of algorithms used in the salt dome model poststack seismic data reconstitution. As it can be seen from the convergence curves, the algorithms have roughly the same convergence trends. In the beginning, the convergence rate of each algorithm is fast and then gradually slows down as the number of iterations increases; The convergence rate of the FIST algorithm is higher than that of the FIHT in the beginning but soon decays to zero, leading to worse relative error of reconstruction results than the FIHT algorithm.

Conclusions

In this paper, two kinds of geophysical data sparse reconstruction algorithms based on *L0*-norm minimization are proposed in this paper with simple computational format and low calculation complexity. Based on the sparseness of the geophysical data or the transform domain, we achieved good reconstruction results for irregular geophysical data by using this algorithm. The choice of the reconstruction algorithm needs to consider the characteristics of the corresponding data: that is, the good continuity of moderate-scale data well suit the iteratively reweighted least-squares algorithm with high convergence rate and short computation, whereas the poor continuity of large-scale data suits the fast iterative hard thresholding algorithm.

It is noteworthy that despite the effort put on geophysical data sparse reconstruction algorithms, most of them are still at the development stage and can only be applied to simple experimental data, whereas actual data are complex, contain various kinds of environmental noise, and their size is much larger than that of the experimental data. Nonetheless, it is critical for geophysical data processing to maintain the efforts of effectively reconstructing irregular actual data.

References

Beck, A., and Teboulle, M., 2009, A fast iterative shrinkage –thresholding algorithm for linear inverse problems: Siam J. Imaging Sciences, **2**(1), 183 – 202.

Bioucas-Dias, J. M., and Figueiredo, M. A. T., 2007, A new twist: two-step iterative shrinkage/thresholding

algorithms for image restoration: IEEE Transactions On Image Processing, **16**(12), 2992 – 3004.

Blumensath, T., and Davies, M. E., 2010, Normalized iterative hard thresholding: guaranteed stability and performance: IEEE Journal of Selected Topics in Signal Processing, **4**(2), 298 – 309.

Blumensath, T., and Davies, M., 2009, Iterative hard thresholding for compressed sensing: Applied and Computational Harmonic Analysis, **27**(3), 265 – 274.

Blumensath, T., 2012, Accelerated iterative hard thresholding: Signal Processing, **92**, 752 – 756.

Candès, E., and Donoho, D., 2000, Curvelets—A surprisingly active nonadaptive representation for objects with edges: Vanderbilt University Press, Nashville, 105 – 120.

Candès, E., and Wakin, M., 2008, An introduction to compressive sampling: IEEE Signal Processing Magazine, **25**(2), 21 – 30.

Cao, J. J., Wang, Y. F., and Yang, C. C., 2012, Seismic data restoration based on compressive sensing using the regularization and zero-norm sparse optimization: Chinese J. Geophys. (in Chinese) **55**(2), 596 – 607.

Donoho, D. L., and Tsaig, Y., 2006, Extensions of compressed sensing: Signal Processing, **86**(3), 533 – 548.

Donoho, D. L., 2006, Compressed sensing: IEEE Transactions on Information Theory, **52**(4), 1289 – 1306.

Duijndam, A. J. W., Schonewille, M. A., and Hindriks, C. O. H., 1999, Reconstruction of band-limited signals, irregularly sampled along one spatial direction : Geophysics, **2**, 524 – 538.

Dunbar, D., and Humphreys, G., 2006, A spatial data structure for poisson-disk sample generation: ACM Transactions on Graphics, **25**(3), 503 – 508.

Guo, L. H., Meng, X. H., and Guo, Z. H., 2005, Gridding methods of geophysical irregular data in space domain: Geophysical & Geochemical Exploration. (in Chinese), **29**(5), 438 – 442.

Hennenfen, G., and Herrmann, F. J., 2008, Simply denoise: wavefield reconstruction via jittered undersampling: Geophysics, **73**(3), 19 – 28.

Herrmann, J., and Hennenfent, G., 2008, Nonparametric seismic data recovery with curvelet frames: Geophysical Journal International, **173**(1), 1 – 5.

Jiao, L. C., Yang, S. Y., and Liu, F., 2011, Development and Prospect of Compressive Sensing: Acta Electronica Sinica, **39**(7), 1651 – 1662.

Levy, S., and Fullagar, P. k., 1981, Reconstruction of a sparse spike train from a portion of its spectrum and application to high-resolution deconvolution: Geophysics, **46**(9), 1235 – 1243.

Li, X., Aravkin, A. Y., and Leeuwen, T. V., 2012, Fast-randomized full-waveform inversion with compressive sensing: Geophysics, **77**(3), 13 – 17.

Liu, X. W., Liu, H., and Liu, B., 2004, A study on algorithm for reconstruction of de-alias uneven seismic data: Chinese J. Geophys. (in Chinese), **47**(2), 299 – 305.

Mallat, S., and Zhang, Z., 1993, Matching pursuit with time-frequency dictionaries: IEEE Trans. on Signal Processing, **41**(12), 3397 – 3415.

Meng, X. H., Hou, J. Q., and Liang, H. Y., 2002, The fast realization of discrete smooth interpolation in the interpolation of potential data: Geophysical & Geochemical Exploration (in Chinese), **26**(4), 302 – 306.

Pei, Y. L., 2009, The method research of sparse constraint deconvolution and wave impedance inversion: Master Thesis Beijing, China University of Geosciences (Beijing).

Qiu, K., and Dogandzic, A., 2012, Sparse signal reconstruction via ECME Hard Thresholding: IEEE Transactions on Signal Processing, **60**(9), 4551 – 4569.

Tang, G., Ma, J. W., and Yang, H. Z., 2012, Seismic data denoising overcomplete based on learning-type overcomplete dictionaries: Applied Geophysics, **9**(1), 27 – 32.

Tang, G., and Yang, H. Z., 2010, Seismic data compression and reconstruction based on poisson disk sampling: Chinese J Geophys (in Chinese), **53**(9), 2181 – 2188.

Tikhonov, A. N., and Arsenin, V. Y., 1977, Solutions of ill-posed problems: John Wiley and Sons, New York.

Trad, D., Ulrych, T., and Sacchi, M., 2003, Latest view of sparse radon transform: Geophysics, **68**(1), 386 – 399.

Tropp, J. A., and Gilbert, A. C., 2007, Signal recovery from random measurements via orthogonal matching pursuit: IEEE Transactions on Information Theory, **53**(12), 4655 – 4666.

Wang, W. Y., and Qiu, Z. Y., 2011, The research to a stable minimum curvature gridding method in potential data processing: Progress in Geophys.(in Chinese), **26**(6), 2003 – 2010.

Chen Guo-Xin is a PhD student at Zhejiang University. He graduated from the College of Mathematics of Shandong University in 2011. His research interests mainly include seismic migration and inversion, and data reconstruction.